American Mineralogist, Volume 98, pages 1906–1913, 2013

Rossiantonite, $Al_3(PO_4)(SO_4)_2(OH)_2(H_2O)_{10}\cdot 4H_2O$, a new hydrated aluminum phosphate-sulfate mineral from Chimanta massif, Venezuela: Description and crystal structure

Ermanno Galli[1], Maria Franca Brigatti[1,*], Daniele Malferrari[1], Francesco Sauro[2,3] and Jo De Waele[2,3]

[1]Dipartimento di Scienze Chimiche e Geologiche, Università di Modena e Reggio Emilia. Largo S. Eufemia 19, I-41121, Modena, Italy
[2]Dipartimento di Scienze Biologiche, Geologiche e Ambientali, Italian Institute of Speleology, Via Zamboni 67, 40126, Bologna, Italy
[3]Associazione di Esplorazioni Geografiche La Venta, Via Priamo Tron 35/F, 31100, Treviso, Italy

Abstract

Rossiantonite, ideally $Al_3(PO_4)(SO_4)_2(OH)_2(H_2O)_{10}\cdot 4H_2O$, triclinic (space group $P\bar{1}$), a = 10.3410(5), b = 10.9600(5), c = 11.1446(5) Å, α = 86.985(2), β = 65.727(2), γ = 75.064(2)°, V = 1110.5(1) Å^3, Z = 2, is a new mineral from the Akopan-Dal Cin cave system in the Chimanta massif (Guyana Shield, Venezuela). The mineral occurs as small (≤0.15 mm) and transparent crystals in a white to slightly pink fine-grained sand, filling spaces between boulders of weathered quartz sandstone. Associated phases are gypsum, sanjuanite, rare alunite, quartz and micro-spherules of amorphous silica.

Rossiantonite is colorless with a white streak and vitreous luster. The mineral is brittle with irregular to sub-conchoidal fracture and it shows a poorly developed cleavage. Rossiantonite is biaxial and not pleochroic, with mean refractive index of 1.504.

The calculated density is 1.958 g/cm^3. Electron microprobe analyses, with H_2O measured by thermogravimetric analysis, provided the following empirical formula based on 28 O apfu: $Al_{2.96}Fe_{0.03}P_{1.01}S_2H_{30.02}O_{28}$. The five strongest lines in the X-ray powder diffraction pattern, expressed as d (Å), I, (hkl) are: 4.647, 100, (210); 9.12, 56, (100); 4.006, 53, (220); 8.02, 40, (110); 7.12, 33, (011).

The crystal structure, refined using 3550 unique reflections to R = 0.0292, is built of PO_4 and Al O_6 polyhedral rings, creating complex chains parallel **b** by sharing the OH-OH edge belonging to the Al(3) polyhedron. Three symmetrically independent Al sites can be identified, namely: Al(1), Al(2), and Al(3). Tetrahedral sites, occupied by P, share all their apexes with AlO_6 octahedra. Unshared octahedral apexes are occupied by water molecules. Four additional water molecules are placed in between the previously identified chains. Two oxygen tetrahedra, occupied by S atoms, are connected along the chains by means of weak hydrogen bonding. The rossiantonite structure shows similarities with minerals belonging to the sanjuanite-destinezite group.

Keywords: Rossiantonite, aluminum-phosphate-sulfate, Chimanta massif, crystal chemistry, crystal structure

Introduction

Rossiantonite is a new mineral species that has been found in the Akopan-Dal Cin cave system, located in the Chimanta massif, a sandstone table mountain of the Guyana Shield outcropping in the protected area of the Canaima National Park (Venezuela). The mineral is genetically closely associated to sanjuanite [$Al_2(PO)_4(SO)_4OH\cdot 9H_2O$] (De Abeledo et al. 1968; Colombo et al. 2011) and shows the same essential chemical elements of hotsonite (Beukes et al. 1984), kribergite (du Rietz 1945), and the unnamed mineral UM1940-01-SO: AlHP (Smith and Nickel 2007). It differs substantially, however, from all of these because of its peculiar stoichiometry.

The mineral is named after Antonio Rossi (1942–2011), professor of Sedimentary Petrology at Modena and Reggio Emilia University and an early developer of scientific speleology in Italy, in recognition of his constant and precious efforts devoted to the study of minerals and, especially, of cave minerals.

The new mineral and mineral name were approved by the Commission on New Minerals, Nomenclature and Classification, IMA no. 2012-056. The holotype material is deposited at the British Museum (registration number BM 2012,99), at the "Museo Mineralogico e Geologico Estense, GEMMA1786" of Modena and Reggio Emilia University, Italy (registration number 2/2012) and at ETH Mineralogical collection (Zurich), catalog number 20130.

Occurrence and paragenesis

The mineral was collected by one of the authors (F.S.) inside the Akopan-Dal Cin cave system in the Akopan Tepui, representing the southern sector of the Chimanta massif (5°10´52´´N 61°57´50´´W; Mecchia et al. 2009). The cave develops inside the quartz sandstone of the Roraima Group. The sedimentary formations of this group show continental to pericontinental facies with an age of approximately 1.8 Ga (Briceño and Schubert 1990; Santos et al. 2003). Low-grade metamorphism, with quartz–pyrophyllite paragenesis in the more arkosic beds, is interpreted as the result of the lithostatic load of the overburden from ~3 km thick sediments, which are now eroded (Urbani 1996). Metamorphism is responsible for quartz overgrowth between the grains thus imparting saccharoidal texture to the

* E-mail: brigatti@unimore.it

0003-004X/13/0010–1906$05.00/DOI: http://dx.doi.org/10.2138/am.2013.4393

quartz sandstone. The cave is hosted by the Mataui Formation, consisting of orthoquartzites and subarkoses with subordinate medium- to fine-grained lithic rocks.

The cave originated from a weathering process involving dissolution of silica cements or quartz grain overgrowths and consequent "arenisation" of the orthoquarzites, piping and mechanical erosion and final removal of the loose quartz grains (Wray 1997; Martini 2000; Sauro et al. 2013).

The sample containing rossiantonite was collected on the floor of a dry passage near the entrance of Cueva Akopan. This sample is a white to slightly pink, fine-grained, light sand, composed of grains of different minerals, between boulders of weathered quartz sandstone. Minerals associated to rossiantonite are gypsum, sanjuanite, rare alunite, quartz, and micro-spherules of amorphous silica. The ceiling above the sampling spot shows many silica speleothems, similar to those described by Aubrecht et al. (2008), probably originating after breaking of the previously mentioned microspherules of amorphous silica.

Physical and optical properties

Rossiantonite forms aggregates of prismatic euhedral crystals, ~0.15 mm in size (Fig. 1). The mineral is colorless and shows a white streak. Crystals are transparent with vitreous luster. Under ultraviolet light, the mineral shows dim green color, regardless of excitation frequency. The tenacity is brittle, the fracture is irregular or sub-conchoidal, and crystals exhibit no cleavage. No twinning is observed. Density and hardness could not be measured because of experimental limitations in separating pure single grains large enough for the purpose. The calculated density is 1.958 g/cm^3 (on the basis of the empirical formula). Rossiantonite dissolves very easily in cold, dilute HCl/H_2O (1:1).

The optical properties could not be fully determined because

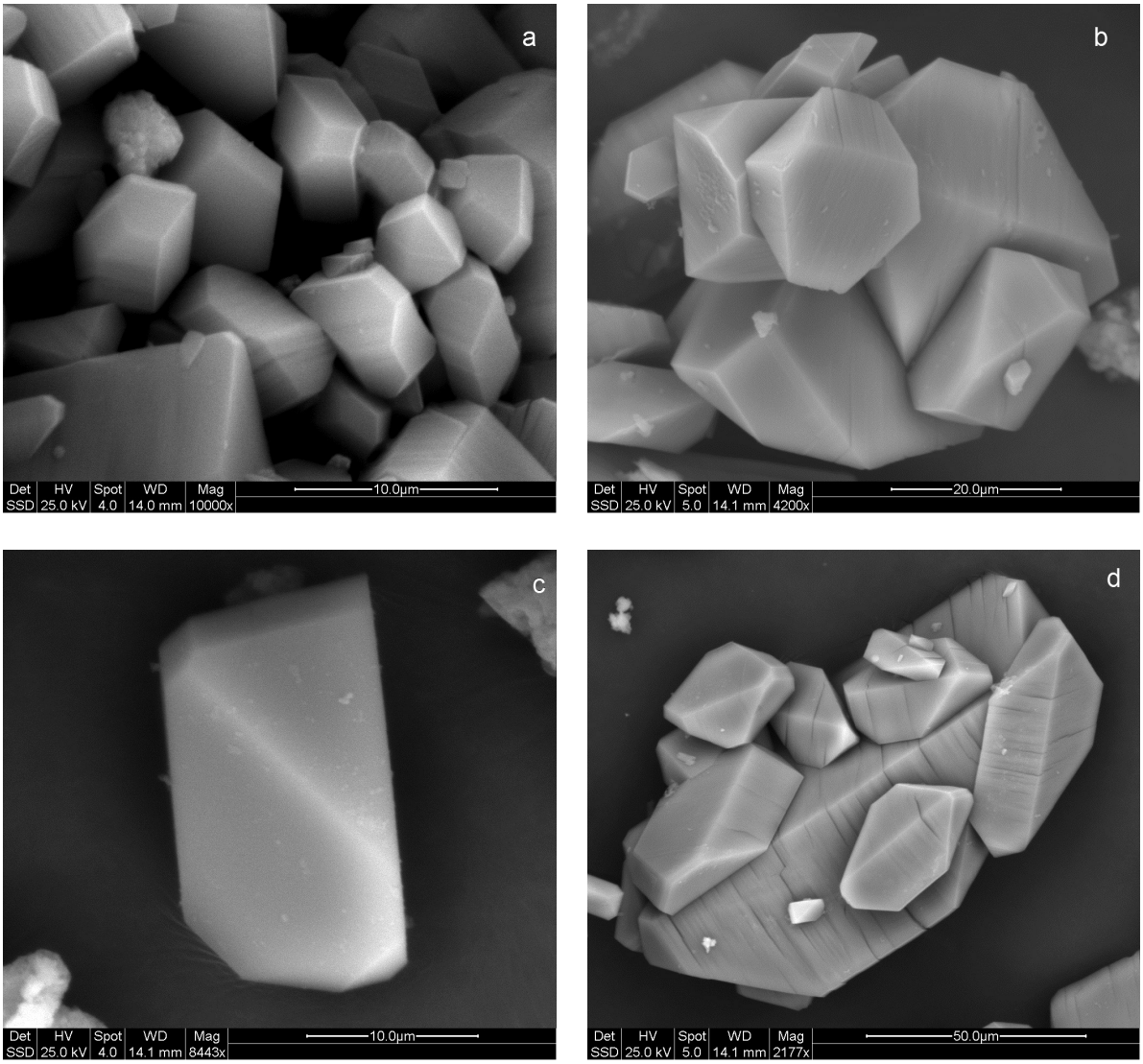

Figure 1. SEM image of rossiantonite from the Akopan-Dal Cin cave system, Chimanta massif, Guyana Shield, Venezuela. (**a** and **b**) crystal aggregates; (**c**) individual crystals; (**d**) crystal aggregates evidencing the damage produced by H_2O loss after exposure to electron beam.

of the small size of the crystals. Under plane-polarized transmitted light, rossiantonite appears moderately birifrangent and not pleochroic with a mean refractive index of $\bar{n}$ = 1.504.

The Gladstone-Dale compatibility index, as defined by Mandarino (1981), provides an assessment of consistency for the average index of refraction, calculated density, and chemical composition. The compatibility index $[1 - (K_P/K_C)]$ for rossiantonite is 0.012 (superior). The mineral is biaxial. Extinction is approximately parallel to the direction of prism elongation and the interference colors vary from light gray to light cyan.

Chemical composition

The chemical composition of rossiantonite was measured with a Cameca SX 50 electron microprobe (EDS mode) on several crystals. A preliminary examination with successive 10 s analytical intervals revealed that the mineral was sensitive to the electron beam, with a monotonic increase in S, P, and Al concentrations with time, possibly because of partial dehydration of the crystals during the experiments. Therefore, the sample was analyzed with a low beam current (2 nA), a scanning beam of 1 μm on both standards and sample and short counting times (10 s). The following standards were used: synthetic Al_2O_3 (Al), synthetic Fe_2O_3 (Fe), barite (S), and apatite (P).

The point analyses from the same fragment and among different fragments were observed to be homogeneous. The value of H_2O = 41.30 wt%, reported in the chemical analysis, was experimentally determined by means of thermogravimetric analysis, including evolved gas mass spectrometry, and thus associated to mass loss specifically related to H_2O.

Degassing under vacuum, following electron beam action in the microprobe chamber, is well documented for hydrated minerals. The sum obtained adding the experimentally determined H_2O value to the oxide percentages is usually greater than 100%. For the investigated mineral, the sum obtained for (Al_2O_3+Fe_2O_3+SO_3+P_2O_5) is 74.96 instead of 58.70 wt%. For this reason the oxide percentages, without water, were recalculated to 58.70 wt%. Recalculation was carried out for all analytical points (11 point analysis) before averaging. Analytical data are given in Table 1.

The empirical formula (based on 28 O apfu) is $Al_{2.96}Fe_{0.03}PS_2H_{30.02}O_{28}$. The structural formula is $Al_3(PO_4)(SO_4)_2(OH)_2(H_2O)_{10}\cdot 4H_2O$, which requires Al_2O_3 = 23.37, P_2O_5 = 10.85, SO_3 = 24.47, H_2O = 41.31, total 100.00 wt%.

Thermal analysis

Thermogravimetry (TG), differential thermal analysis (DTA), and derivative thermogravimetric curves (Fig. 2a) were obtained simultaneously and were performed with a Seiko SSC 5200 thermal analyzer equipped with a quadrupole mass spectrometer (ESS, GeneSys Quadstar 422) to analyze gases evolved during thermal reactions. This device samples gases via an inert, fused silicon capillary system, heated to prevent gas condensing. Analyses of evolved gas phases were carried out in multiple ion detection mode (MID), which allows the qualitative determination of evolved masses vs. temperature or time. The ion current curves of the evolved phases are shown in Figure 2b. The heating rate and the temperature range were set at 10 °/min and 20–1200 °C, respectively. The total weight loss was 64.8%. Two ranges of weight loss can be identified from the TG curve: the first interval (20–500 °C) evidences a very strong endothermic reaction with a maximum at 149 °C attributed to water molecules only, as confirmed by mass spectrometry. The related weight loss is 41.30 wt%. The second interval shows a reaction at 719 °C, connected to the formation of $Al_2(SO_4)_3$ (millosevichite-like structure), as indicated by powder X-ray diffraction on sample heated at 780 °C, and a strong maximum at 975 °C, giving a reduction of 21.0 wt%, associated to the release of SO_2 (Figs. 2). The endo-exothermic reaction between 975 and 1100 °C corresponds to the formation of $AlPO_4$ (berlinite-like structure). All these conclusions were confirmed by XRD analysis on phases generated after each thermal reaction.

Table 1. Chemical composition of rossiantonite

Constituent	wt%	Range	σ
Al_2O_3	23.07	22.72–23.41	0.16
Fe_2O_3	0.30	0.17–0.50	0.01
SO_3	24.44	23.92–24.93	0.11
P_2O_5	10.89	10.60–11.09	0.02
H_2O	41.30		
Total	100.00		

Note: The wt% were recalculated to match results from microprobe and thermal analysis. See text for details. σ = standard deviation.

Infrared spectroscopy

Infrared spectra were recorded with an ATR Golden Gate (BRUKER - VERTEX 70) in the range 4000–600 cm^{-1} (Fig. 3).

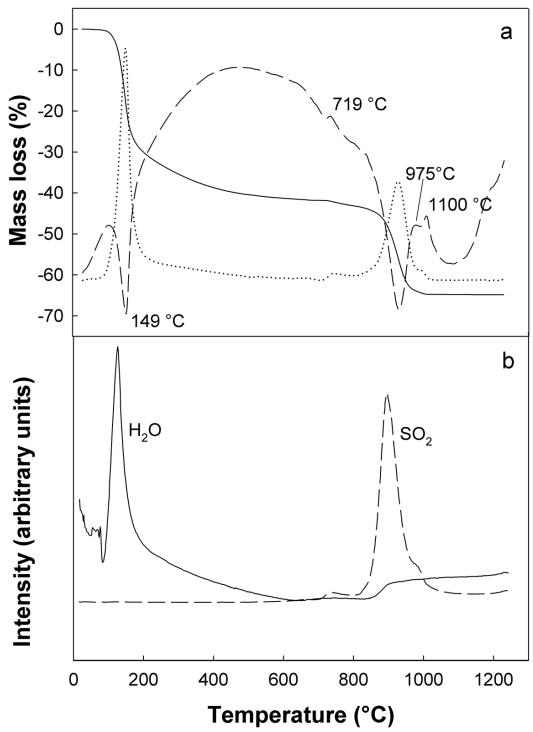

Figure 2. (**a**) Thermogravimetric (solid line), derivative thermogravimetric (dotted line), and thermodifferential (dashed line) curves for rossiantonite. (**b**) Mass spectra of evolved gases during thermal analysis. Solid line H_2O (mass/charge ratio 18 uma); dashed line SO_2 (mass/charge ratio 64 uma).

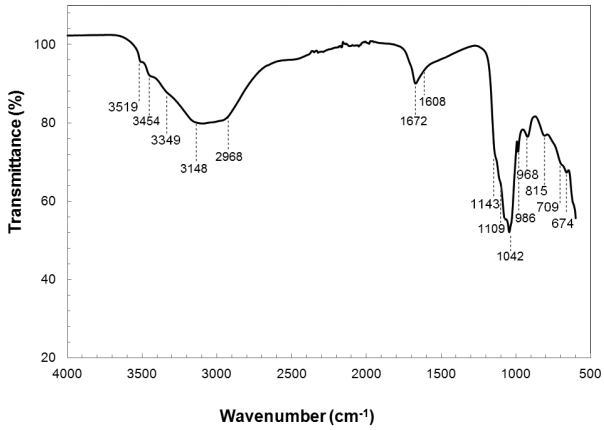

FIGURE 3. Infrared spectrum of rossiantonite in the range 4000–600 cm^{-1}.

The mineral contains four vibrational spectroscopically distinct units, namely phosphate, sulfate, and hydroxyl units as well as water. Each one of these groups shows its own characteristic spectrum. The infrared spectrum of the hydroxyl stretching region (2400–3800 cm^{-1}) of rossiantonite is complex with a series of overlapping bands.

In the region 2400–3800 cm^{-1}, infrared bands are observed at 2968, 3148, 3349, 3454, and 3519 cm^{-1}. The band at 3519 cm^{-1} can be assigned to the OH stretching vibration of the hydroxyl units. The effects at 3454, 3349, and 3148 cm^{-1} are related to the stretching mode $\nu_3(H_2O)$ of the two types of H_2O in the structure (i.e., H_2O related to Al-centered octahedra and H_2O between tetrahedral and octahedral chains). The band at a lower wavenumber (2968 cm^{-1}) is attributed to strongly hydrogen-bonded water (Frost and Palmer 2011).

The shoulder at 1608 and the band at 1672 cm^{-1} represent weakly hydrogen and strongly hydrogen bonded water (Frost and Palmer 2011). In the region 650–1200 cm^{-1}, the spectrum

TABLE 2. X-ray powder diffraction data for rossiantonite

I_{rel}	2θ	d_{obs}	d_{calc}	*hkl*	I_{rel}	2θ	d_{obs}	d_{calc}	*hkl*
11	8.34	10.61	10.57	0 1 0	4	34.458	2.603	2.602	2 $\bar{1}$ 4, $\bar{1}$ $\bar{4}$ 1
32	8.71	10.16	10.14	0 0 1	2	35.357	2.539	2.536	4 1 1
56	**9.69**	**9.12**	**9.11**	**1 0 0**	1	35.602	2.522	2.523	3 0 4, 3 $\bar{2}$ 1, 0 4 1
10	10.00	8.84	8.82	1 0 1	4	35.927	2.500	2.500	0 $\bar{1}$ 4, 4 0 2, 2 4 2
40	**11.04**	**8.02**	**8.00**	**1 1 0**	4	36.373	2.470	2.471	1 4 2, 4 1 3
16	11.70	7.56	7.55	0 $\bar{1}$ 1	3	36.362	2.432	2.433	0 1 4, 1 $\bar{2}$ 4
33	**12.43**	**7.12**	**7.11**	**0 1 1**	1	37.194	2.417	2.417	$\bar{3}$ 1 1
2	14.31	6.19	6.19	1 $\bar{1}$ 1	3	37.406	2.404	2.403	0 $\bar{4}$ 2, 1 $\bar{4}$ 1, 4 0 3
22	15.50	5.72	5.71	$\bar{1}$ 0 1	2	37.768	2.382	2.378	1 $\bar{4}$ 0
6	16.11	5.50	5.49	1 0 2	3	38.305	2.350	2.347	3 4 2
2	16.74	5.30	5.28	0 2 0	4	38.631	2.331	2.332	$\bar{2}$ $\bar{1}$ 3
3	17.49	5.07	5.07	1 1 2	3	39.327	2.291	2.287	0 4 2
29	17.74	5.00	4.99	2 0 1, 1 2 1	2	39.573	2.277	2.277	4 0 0
12	18.423	4.816	4.806	0 $\bar{2}$ 1	4	39.895	2.260	2.257	4 $\bar{1}$ 1
100	**19.101**	**4.647**	**4.642**	**2 1 0**	3	40.303	2.238	2.239	4 3 3, $\bar{1}$ 4 1, 0 2 4
14	19.371	4.582	4.575	0 2 1	3	40.562	2.224	2.224	$\bar{1}$ $\bar{1}$ 4
5	19.834	4.476	4.469	0 1 2	2	41.21	2.191	2.193	3 4 3, 1 4 3, 1 5 0
2	20.111	4.416	4.408	2 0 2	2	41.716	2.165	2.162	$\bar{2}$ $\bar{4}$ 2
3	20.503	4.332	4.324	$\bar{1}$ $\bar{2}$ 1	2	42.309	2.136	2.136	1 $\bar{1}$ 5, 1 1 5
7	21.110	4.209	4.202	$\bar{2}$ 2 1	2	42.984	2.103	2.101	4 4 2, $\bar{2}$ $\bar{3}$ 3
7	21.495	4.134	4.126	2 $\bar{1}$ 1, 1 $\bar{2}$ 0	3	43.192	2.095	2.095	0 $\bar{5}$ 1, $\bar{3}$ 1 2
53	**22.190**	**4.006**	**4.001**	**2 2 0**	3	43.826	2.066	2.065	2 $\bar{4}$ 0
18	23.149	3.842	3.836	2 $\bar{1}$ 0	<1	44.798	2.023	2.025	4 4 3
27	23.321	3.814	3.808	2 $\bar{1}$ 2, $\bar{1}$ 0 2	10	45.285	2.003	2.002	0 3 4, 5 1 1
28	23.528	3.781	3.774	2 2 2, 0 $\bar{2}$ 2	2	46.112	1.969	1.966	$\bar{1}$ 2 4
5	23.960	3.712	3.706	1 0 3, $\bar{2}$ $\bar{1}$ 1	3	46.858	1.939	1.937	5 0 1, $\bar{3}$ $\bar{1}$ 3, $\bar{2}$ 4 1
12	24.468	3.638	3.633	$\bar{2}$ 0 1	1	47.443	1.915	1.915	3 $\bar{3}$ 4, 3 $\bar{2}$ 3
15	25.235	3.529	3.523	0 3 0, 1 3 1	2	47.646	1.909	1.907	$\bar{2}$ 0 4
8	25.501	3.493	3.487	2 0 3	4	48.405	1.881	1.881	4 $\bar{1}$ 5
9	25.749	3.460	3.455	2 1 3	3	49.098	1.856	1.857	0 2 5, 2 0 6, $\bar{4}$ $\bar{4}$ 1
12	25.991	3.428	3.423	$\bar{1}$ 1 2	2	50.023	1.823	1.827	$\bar{1}$ 0 5
15	26.372	3.380	3.381	0 0 3, $\bar{2}$ $\bar{2}$ 1	2	50.491	1.808	1.805	$\bar{1}$ $\bar{4}$ 4
5	26.587	3.353	3.352	3 1 2	1	51.041	1.789	1.790	2 $\bar{5}$ 1, $\bar{1}$ 3 4, $\bar{1}$ $\bar{2}$ 5
9	27.200	3.279	3.278	0 $\bar{1}$ 3	6	51.932	1.761	1.761	2 6 2
2	27.487	3.245	3.240	2 $\bar{2}$ 1	2	53.244	1.719	1.718	0 6 1, 6 2 3
5	27.742	3.216	3.217	$\bar{2}$ 1 1	2	53.485	1.713	1.712	$\bar{2}$ 2 4
3	28.454	3.137	3.133	3 2 2	3	54.39	1.687	1.685	0 $\bar{1}$ 6
7	28.815	3.098	3.097	1 3 2	2	55.083	1.667	1.668	5 $\bar{2}$ 4, 2 6 3
4	29.412	3.037	3.036	3 0 0	<1	55.553	1.654	1.655	4 3 6, 0 1 6, $\bar{3}$ $\bar{2}$ 4
24	29.888	2.990	2.988	3 2 0	<1	56.109	1.639	1.638	5 1 6, $\bar{2}$ $\bar{1}$ 5
9	30.335	2.947	2.942	3 $\bar{1}$ 1	3	57.413	1.605	1.607	$\bar{4}$ 0 3, 3 5 5, $\bar{2}$ 4 3
5	30.769	2.906	2.903	$\bar{2}$ $\bar{1}$ 2	<1	58.3	1.583	1.583	0 2 6, 2 5 5
4	31.345	2.854	2.850	1 $\bar{3}$ 2	1	59.036	1.563	1.563	5 $\bar{1}$ 2
21	31.849	2.810	2.807	3 3 1	1	59.25	1.560	1.559	2 $\bar{1}$ 7, 2 7 1, $\bar{2}$ 5 2, $\bar{2}$ $\bar{3}$ 5
2	32.328	2.769	2.765	$\bar{1}$ 3 1	<1	60.096	1.540	1.539	4 $\bar{4}$ 0
4	32.569	2.749	2.747	$\bar{2}$ $\bar{2}$ 2	2	60.764	1.523	1.524	$\bar{4}$ $\bar{4}$ 3
4	33.524	2.673	2.673	1 1 4	2	60.99	1.519	1.518	3 7 0
7	34.085	2.630	2.630	$\bar{1}$ $\bar{2}$ 3, 2 4 1	2	61.428	1.509	1.510	0 7 0, 6 5 2

Note: Estimated standard deviations on the observed 2θ-values are ~2% of reported values. Lines in bold identify strongest reflections.

is dominated by the band at 986 cm^{-1} assigned to the $(PO_4)^{3-}$ ν_1 symmetric stretching band. The band observed at 1042 cm^{-1} is assigned to the $(SO_4)^{2-}$ ν_1 symmetric stretching mode. As observed by Frost and Palmer (2011), the sulfate and phosphate stretching modes are possibly coupled, thus giving the intense band at 986 cm^{-1}. The bands at 1109 and 1143 cm^{-1} are attributed to the ν_3 antisymmetric stretching modes of $(PO_4)^{3-}$ and $(SO_4)^{2-}$. These values match data reported for other phosphate-sulfate minerals well (Colombo et al. 2011). Bands at 709 and 674 cm^{-1} are associated to vibrational modes involving H_2O molecules in a crystalline environment (Assaoudi and Ennaciri 1997). The sharp band at 1042 cm^{-1} and that at 815 cm^{-1} are related to $\nu_3(PO_4)^{3-}$ and to Al-O-P antisymmetric stretching, respectively.

X-ray diffraction

Powder diffraction

The X-ray powder-diffraction pattern (Table 2) was recorded on a PANalytical X'Pert PRO diffractometer using monochromatic Cu$K\alpha_1$ radiation and calibrated with silicon as internal standard. Reflections were indexed using the results of the single-crystal study. The intensities of calculated powder lines, based on the structure determination, demonstrate generally good agreement between the observed and calculated patterns. Similarly, unit-cell parameters, refined by whole pattern least-squares refinement confirmed a triclinic cell with a = 10.3415(3), b = 10.9580(3), c = 11.1445(3) Å, α = 86.968(4), β = 65.757(3), γ = 75.055(3)°, V = 1110.57(4) Å^3 in close agreement with parameters obtained from the single-crystal study.

Single-crystal diffraction

Some rossiantonite crystals, optically homogeneous and inclusion-free, were selected for single-crystal X-ray study and analyzed with a Bruker X8 APEX four circle diffractometer combined with an APEX 4 K CCD detector, flat graphite monochromator and Mo$K\alpha$-radiation from a fine focus sealed tube. Unit-cell dimensions, determined by least-squares refinement of the setting angles of 25 high-θ reflections ($15 < \theta < 22°$), show nearly identical values for the various investigated crystals. The data collection was carried out on the crystal showing the best diffraction quality. The SMART program suite was used for unit-cell determination and X-ray data collection. Redundant data were collected for an approximate sphere of reciprocal space and processed using the Bruker AXS program SAINT+ (Bruker 1999). A Gaussian absorption correction was performed using a linear absorption coefficient (μ) of 1.90 mm^{-1}. The absorption correction, space group determination, and data merging were performed using XPREP, a part of the SHELX-97 software package (Sheldrick 1997). The details of the data collection and the final structure refinement are provided in Table 3.

The structure was solved by direct methods using SIR2004 (Burla et al. 2005). SHELXL-97 software (Sheldrick 2008) was used, with neutral atom scattering factors, for the refinement of the structure. The E statistics indicate that the structure is centrosymmetric. The structure was solved and refined in space group $P\bar{1}$. Direct methods provided the locations of all cation sites and of several O sites. The other O sites and all H sites were located on difference-Fourier maps.

The structure was refined by a combination of least-squares refinement and difference-Fourier synthesis to an R index of 0.0292 using soft constraints for the O–H distances. The maximum and minimum residual electron-density peaks are 0.52 and –0.27 e/Å^{-3}, respectively. Final atomic parameters are listed in Table 4, and selected interatomic distances are given in Table 5. Table 6[1] gives bond-valence values calculated from the parameters of Brown and Altermatt (1985).

Description of the structure

Overview of structure topology

Figure 4a represents a projection of the polyhedral structure down the **c***. Figure 4b details the chain developing along **b**. From these images it is well evident that the rossiantonite structure is dominated by chains extending parallel to **b**.

The repeating subunit of the chain consists of three symmetry-independent AlX_6 octahedra (X = O, OH, H_2O) and a PO_4 tetrahedron. $Al(1)X_6$ and $Al(2)X_6$ octahedra share a common vertex [i.e., O(5)h)]. The PO_4 tetrahedron shares one vertex with Al(2) and Al(3) octahedra, i.e., O2 and O1 anion sites, respectively, and two vertices with the Al(1) octahedron [i.e., O(3) and O(4) anions] forming three-membered polyhedral rings. These rings form ideally infinite chains by sharing one edge [i.e., O(13)h-O(13)h octahedral edge], of two adjacent Al(3) octahedra (Fig. 4b). The structure is completed by two symmetrically independent SO_4 tetrahedra and by four H_2O sites (Fig. 4a).

The topology of the chain in rossiantonite appears to be unique, based on our review on sulfate and phosphate structures. However the pattern, where a tetrahedron occupied by P forms 3-membered ring subunits with octahedra occupied by Al,

[1] Deposit item AM-13-1009, Table 6 and CIF. Deposit items are stored on the MSA web site and available via the *American Mineralogist* Table of Contents. Find the article in the table of contents at GSW (ammin.geoscienceworld.org) or MSA (www.minsocam.org), and then click on the deposit link.

Table 3. Data collection and structure refinement details for rossiantonite

Crystal size (mm)	0.12 × 0.07 × 0.03
Diffractometer	Bruker X8 APEX
X-ray radiation/power	Mo$K\alpha$ (λ = 0.71075 Å)/30 kV, 52 mA
Temperature (K)	298(2)
Structural formula	$Al_3(PO_4)(SO_4)_2(OH)_2(H_2O)_{10}\cdot 4H_2O$
Space group	$P\bar{1}$
Unit-cell dimensions	a = 10.3410(5) Å
	b = 10.9600(5) Å
	c = 11.1446(5) Å
	α = 86.985(2)°
	β = 65.727(2)°
	γ = 75.064(2)°
Volume (Å^3)	1110.5(1)
Z	2
Measured reflections	15073
Reflection with $I > 2\sigma(I)$	3550
Refined parameters	438
θ range	1.93–24.25°
Index ranges	$-11 \le h \le +11$
	$-12 \le k \le +12$
	$-12 \le l \le +10$
Completeness to θ = 24.25° (%)	99.1
R_{int}	0.0449
Refinement method	Full-matrix least-squares on F^2
R [$F^2 > 2\sigma(I)$]	0.0292
wR (F^2)	0.0643
Goodness of fit	0.944

TABLE 4. Fractional coordinates and atom displacement parameters ($Å^2 \times 10^3$)

Atom	x	y	z	U_{eq}	U_{11}	U_{22}	U_{33}	U_{23}	U_{13}
P	0.5169(1)	0.6628(1)	0.0611(1)	12(1)	13(1)	11(1)	12(1)	1(1)	−5(1)
Al(1)	0.2508(1)	0.6175(1)	0.0287(1)	12(1)	12(1)	11(1)	13(1)	0(1)	−6(1)
Al(2)	0.2686(1)	0.6219(1)	0.3303(1)	14(1)	14(1)	16(1)	13(1)	2(1)	−6(1)
Al(3)	0.5557(1)	0.9431(1)	0.0933(1)	13(1)	15(1)	13(1)	14(1)	1(1)	−7(1)
S(1)	0.9545(1)	0.0474(1)	0.2582(1)	19(1)	18(1)	20(1)	17(1)	0(1)	−7(1)
S(2)	0.7454(1)	0.6453(1)	0.3275(1)	17(1)	16(1)	17(1)	16(1)	2(1)	−7(1)
O(1)	0.5849(2)	0.7740(2)	0.0446(2)	15(1)	14(1)	12(1)	18(1)	1(1)	−7(1)
O(2)	0.4415(2)	0.6399(2)	0.2062(2)	17(1)	14(1)	24(1)	15(1)	2(1)	−6(1)
O(3)	0.4034(2)	0.6926(2)	0.0003(2)	15(1)	17(1)	14(1)	18(1)	3(1)	−10(1)
O(4)	0.3621(2)	0.4525(2)	0.0155(2)	17(1)	14(1)	12(1)	20(1)	−1(1)	−4(1)
O(5)h	0.1804(2)	0.6365(2)	0.2137(2)	17(1)	12(1)	22(1)	15(1)	1(1)	−4(1)
O(6)w	0.1251(2)	0.7794(2)	0.0270(2)	23(1)	26(1)	21(1)	20(1)	−5(1)	−14(1)
O(7)w	0.6929(2)	0.3868(2)	0.1600(2)	22(1)	29(1)	19(1)	18(1)	−1(1)	−11(1)
O(8)w	0.0937(2)	0.5460(2)	0.0478(2)	21(1)	16(1)	21(1)	26(1)	−1(1)	−8(1)
O(9)w	0.1113(2)	0.5784(2)	0.4734(2)	20(1)	16(1)	22(1)	18(1)	6(1)	−3(1)
O(10)w	0.1735(2)	0.7943(2)	0.3898(2)	23(1)	34(1)	17(1)	18(1)	−1(1)	−15(1)
O(11)w	0.3450(3)	0.4378(2)	0.2952(3)	25(1)	24(1)	19(1)	25(1)	1(1)	−4(1)
O(12)w	0.3621(2)	0.6150(2)	0.4500(2)	22(1)	20(1)	30(1)	17(1)	9(1)	−9(1)
OH(13)h	0.3809(2)	1.0061(2)	0.0768(2)	16(1)	10(1)	20(1)	16(1)	4(1)	−3(1)
O(14)w	0.4662(3)	0.9136(2)	0.2753(2)	23(1)	27(1)	17(1)	18(1)	−1(1)	−8(1)
O(15)w	0.7472(2)	0.8864(2)	0.0953(2)	21(1)	22(1)	18(1)	27(1)	5(1)	−14(1)
O(16)w	0.5546(2)	1.1076(2)	0.1525(2)	25(1)	43(1)	17(1)	24(1)	4(1)	−21(1)
O(17)	0.0988(2)	1.0009(2)	0.2612(2)	38(1)	24(1)	48(1)	39(1)	14(1)	−13(1)
O(18)	0.9536(2)	1.1532(2)	0.1728(2)	38(1)	40(1)	46(1)	39(1)	21(1)	−25(1)
O(19)	0.9144(2)	0.9463(2)	0.2116(2)	41(1)	41(1)	34(1)	44(1)	−15(1)	−14(1)
O(20)	0.8423(2)	0.0913(2)	0.3931(2)	29(1)	29(1)	33(1)	21(1)	−7(1)	−7(1)
O(21)	0.8065(2)	0.6617(2)	0.1846(2)	22(1)	22(1)	24(1)	16(1)	4(1)	−6(1)
O(22)	0.6712(2)	0.5414(2)	0.3532(2)	25(1)	32(1)	26(1)	27(1)	8(1)	−17(1)
O(23)	0.6333(2)	0.7620(2)	0.3965(2)	27(1)	25(1)	25(1)	21(1)	−4(1)	−6(1)
O(24)	0.8619(2)	0.6151(2)	0.3743(2)	25(1)	24(1)	29(1)	30(1)	10(1)	−18(1)
W(1)	0.1245(3)	0.3117(2)	0.1365(2)	29(1)	25(1)	27(1)	31(1)	−3(1)	−5(1)
W(2)	0.2845(3)	1.0876(2)	0.4652(2)	33(1)	39(1)	30(1)	24(1)	−1(1)	−5(1)
W(3)	0.4048(3)	0.7884(2)	0.6555(2)	31(1)	28(1)	43(1)	20(1)	−4(1)	−10(1)
W(4)	0.1551(2)	0.2942(2)	0.3651(2)	31(1)	32(1)	30(1)	28(1)	−3(1)	−12(1)
H(5)	0.110(3)	0.631(3)	0.247(3)	24(11)					
H(6)	0.896(3)	1.198(3)	0.036(3)	40(11)					
H(6′)	0.072(3)	0.825(3)	0.094(3)	25(9)					
H(7)	0.700(4)	0.436(3)	0.204(4)	59(13)					
H(7′)	0.672(4)	0.331(4)	0.205(4)	59(14)					
H(8)	0.004(4)	0.583(3)	0.082(3)	40(11)					
H(8′)	0.102(3)	0.466(3)	0.075(3)	47(11)					
H(9)	0.122(4)	0.510(3)	0.518(3)	54(11)					
H(9′)	0.027(4)	0.625(4)	0.528(4)	73(14)					
H(10)	0.168(3)	0.826(3)	0.455(3)	33(10)					
H(10′)	0.156(3)	0.849(3)	0.342(3)	38(10)					
H(11)	0.290(4)	0.390(3)	0.312(3)	51(13)					
H(11′)	0.392(4)	0.426(3)	0.230(3)	38(13)					
H(12)	0.458(4)	0.602(3)	0.414(3)	54(12)					
H(12′)	0.347(3)	0.567(3)	0.506(3)	31(10)					
H(13)	0.302(3)	1.009(3)	0.127(3)	22(9)					
H(14)	0.513(4)	0.864(3)	0.303(3)	53(13)					
H(14′)	0.417(3)	0.967(3)	0.328(3)	26(10)					
H(15)	0.757(4)	0.819(4)	0.124(3)	45(13)					
H(15′)	0.783(4)	0.930(4)	0.120(4)	64(14)					
H(16)	0.561(4)	1.136(3)	0.217(4)	57(12)					
H(16′)	0.571(3)	1.171(3)	0.102(3)	38(10)					
HW1	1.072(3)	1.259(3)	0.144(3)	38(10)					
HW1′	0.215(4)	0.274(3)	0.075(4)	56(12)					
HW2	0.222(3)	0.043(3)	0.525(3)	46(10)					
HW3	0.332(4)	0.823(4)	0.635(4)	73(14)					
HW3′	0.471(4)	0.763(3)	0.587(4)	42(12)					
HW4	0.143(4)	0.286(3)	0.296(4)	65(13)					
HW4′	0.186(4)	0.223(4)	0.401(4)	73(13)					

Notes: Labels: P = phosphorous site; Al(1), Al(2), Al(3) = three symmetrically independent aluminum sites; S = sulfur site; O = anionic oxygen sites; H = hydrogen sites; W = oxygen position related to free H_2O. Label h identifies octahedral OH sites, label w identifies octahedral sites occupied by H_2O. Standard deviation in parentheses.

constituting chains, is observed in other sulfate and phosphate structures, such as those of destinezite and sanjuanite (Peacor et al. 1999; Colombo et al. 2011).

Cation sites

The rossiantonite polyhedral structure is constituted by a tetrahedrally coordinated P position, by two tetrahedrally coordinated S [(S(1) and S(2)] positions, and by three symmetrically distinct octahedrally coordinated Al positions, namely Al(1), Al(2), and Al(3).

The P site is completely occupied by P and coordinated by four O atoms, i.e., O(1), O(2), O(3), O(4), showing an average ⟨P-O⟩ distance of 1.527 Å [range 1.520(2)–1.542(2) Å, Table 5], which is similar to the average ⟨P-O⟩ distance of 1.537 (range

TABLE 5. Selected bond distances (Å) in rossiantonite

P–O(1)	1.524(2)	S(1)–O(17)	1.461(2)	S(2)–O(21)	1.472(2)
P–O(2)	1.520(2)	S(1)–O(18)	1.461(2)	S(2)–O(22)	1.484(2)
P–O(3)	1.542(2)	S(1)–O(19)	1.465(2)	S(2)–O(23)	1.476(2)
P–O(4)	1.520(2)	S(1)–O(20)	1.481(2)	S(2)–O(24)	1.458(2)
<P–O>	1.527	<S(1)–O>	1.467	<S(2)–O>	1.473
Al(1)–O(3)	1.871(2)	Al(2)–O(2)	1.807(2)	Al(3)–O(1)	1.872(2)
Al(1)–O(4)	1.853(2)	Al(2)–O(5)h	1.851(2)	Al(3)–O(13)h	1.842(2)
Al(1)–O(5)h	1.887(2)	Al(2)–O(9)w	1.899(2)	Al(3)–O(13)h′	1.843(2)
Al(1)–O(6)w	1.915(2)	Al(2)–O(10)w	1.902(2)	Al(3)–O(14)w	1.902(2)
Al(1)–O(7)w	1.937(2)	Al(2)–O(11)w	1.964(2)	Al(3)–O(15)w	1.925(2)
Al(1)–O(8)w	1.911(2)	Al(2)–O(12)w	1.932(2)	Al(3)–O(16)w	1.948(2)
<Al(1)–O>	1.896	<Al(2)–O>	1.893	<Al(3)–O>	1.889
		O–H bonds			
O(5)h–H(5)	0.69(2)	O(11)w–H(11)	0.83(3)	W(1)–H(W1)	0.90(3)
O(6)w–H(6)	0.82(3)	O(11)w–H(11)	0.68(3)	W(1)–H(W1)′	0.88(3)
O(6)w–H(6)′	0.82(2)	O(12)w–H(12)	0.88(3)	W(2)–H(W2)	0.93(3)
O(7)w–H(7)	0.78(3)	O(12)w–O(12)′	0.78(3)	W(2)–(W2)′	0.83(3)
O(7)w–H(7)′	0.79(3)	O(13)h–H(13)	0.77(3)	W(3)–H(W3)	0.79(4)
O(8)w–H(8)	0.84(3)	O(14)w–H(14)	0.77(3)	W(3)–H(W3)′	0.86(4)
O(8)w–H(8)′	0.90(3)	O(14)w–H(14)′	0.76(3)	W(4)–H(W4)	0.84(3)
O(9)w–H(9)	0.89(3)	O(15)w–H(15)	0.79(4)	W(4)–H(W4)′	0.90(3)
O(9)w–H(9)′	0.87(3)	O(15)w–H(15)′	0.80(4)		
O(10)w–H(10)	0.80(3)	O(16)w–H(16)	0.83(3)		
O(10)w–H(10)′	0.82(3)	O(16)w–H(16)′	0.88(3)		

1.439–1.625 Å) given by Huminicki and Hawthorne (2002) for well-refined phosphate minerals. Bond valence calculations (Table 6[1]) and bond lengths (Table 5) strongly indicate a complete occupancy of this site by P.

Bond-length and bond-valence values suggest that the Al(1) octahedron [Al(1)O_2(OH)(H_2O)$_3$] is coordinated by two oxygen atoms [O(3) and O(4)] shared with a PO_4 tetrahedron, by an OH group, i.e., O(5)h, shared with the Al(2) octahedron and by three water molecules at the unshared corners, i.e., O(6)w, O(7)w, and O(8)w positions (Tables 5 and 6[1]). The ⟨Al(1)-O⟩ distance is 1.896 Å, with bond lengths ranging from 1.853(2) to 1.937(2) Å. The Al(1) complex coordination pattern produces a distorted polyhedron (bond length distortion, BLD = ⟨[(Al-O)$_i$ – ⟨Al-O⟩]⟩/⟨Al-O⟩×100 = 1.34). The three longer distances are related to Al(1)-OH_2 bonds.

The Al(2) octahedron [Al(2)O(OH)(H_2O)$_4$] is coordinated by one oxygen atom [O(2)] shared with the PO_4 tetrahedron, one OH group [O(5)h] that is shared with the Al(1) octahedron, as previously indicated, and by four H_2O molecules, namely O(9)w, O(10)w, O(11)w, and O(12)w positions. The ⟨Al(2)-O⟩ is 1.893 Å, with bond lengths ranging from 1.807(2) to 1.964(2) Å and BLD = 2.34%.

The Al(3) octahedron [Al(3)O(OH)$_2$(H_2O)$_3$] is coordinated by one oxygen atom [O(1)] shared with the PO_4 tetrahedron, by two OH group [O(13)h], which constitute the edge shared between two adjacent Al(3) octahedra, and by three water molecules, namely O(14)w, O(15)w and O(16)w. The ⟨Al(3)-O⟩ distance is 1.889 Å, with bond lengths ranging from 1.842(2) to 1.948(2) Å. The calculated BLD is 1.92%. The octahedron showing greatest distortion is Al(2), which is also characterized by sharing four water molecules instead of three, as observed for Al(1) and Al(3).

The structure contains two S sites, i.e., S(1) and S(2) coordinated by four oxygen atoms in a quite regular tetrahedral arrangement. ⟨S-O⟩ distances are 1.467 Å (range 1.461–1.481 Å) and 1.473 Å (range 1.458–1.484 Å), for S(1) and S(2) tetrahedra, respectively. These values are in agreement with the average ⟨S-O⟩ length of 1.473 Å commonly observed for a sulfate ion (Louisnathan et al. 1977). Bond valence calculation and bond lengths are consistent with the complete occupancy of the site by S. Each S polyhedron is surrounded by H ions with distances from its apices ranging from approximately 1.79 to 1.95 Å. Hydrogen atoms are coordinated to octahedral oxygen atoms, forming OH and H_2O groups.

Possible origin of rossiantonite

The origin of sulfates and rare sulfates-phosphates in the quartz sandstone caves of the tepuis is discussed by Sauro et al. (2013). However the origin of rossiantonite is still not clear. The mineralogical association (gypsum, alunite, sanjuanite) is very similar to that described for the sanjuanite occurrence in

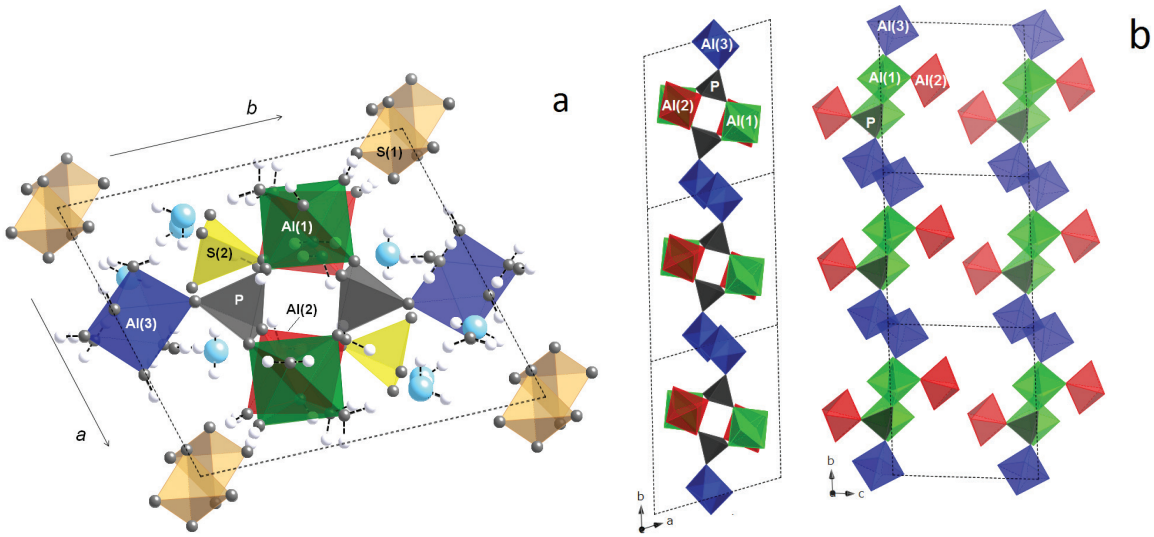

FIGURE 4. (**a**) Projection of the structure along [001]. Filled polyhedra: green [Al(1)], red [Al(2)], blue [Al(3)], gray (P), orange [S(1)], and yellow [S(2)]. Spheres: gray (oxygen atoms), light blue (water molecules), and white (hydrogen atoms). Hydrogen bonds are shown as thin black dashed lines. (**b**) Chain development in the structure. S polyhedra and water molecules were omitted.

Argentina (De Abeledo et al. 1968), developing however under remarkably different environments: Carboniferous-Ordovician limestone bedrock and arid climate, in Argentina, and Precambrian quartz sandstone under tropical wet conditions, in Venezuela. De Abeledo et al. (1968) suggested a hydrothermal origin for sanjuanite with ascending acidic solutions. Colombo et al. (2011) suggested instead that the origin of sulfur in sanjuanite could be related to the weathering under arid conditions of syngenetic sulfides like pyrite in pelites or in Fe^{3+} oxy-hydroxide veins.

In the case of rossiantonite, WDS analyses demonstrated that the residual "red muds," consisting of Fe^{3+} oxy-hydroxides (hematite and goethite), observed along the wall and on the floor of the cave, are almost completely depleted in sulfur (below 10 ppm) and therefore cannot be considered the source for this element. On the other hand isotopic data on sulfur and oxygen from sulfates and sulfates-phosphates collected in many quartz sandstone caves of Venezuelan tepuis (for a detailed discussion and data see Sauro et al. unpublished manuscript) suggest that sulfur originates from marine spray from the Atlantic Ocean, with possible contributions of dimethyl sulfide (DMS) and microbially reduced sulfur from the forests or peatbogs within the watershed. This spray, after having been conveyed inside the caves for hundreds of thousands of years following air currents, may thus account for the formation of sulfates and sulfates-phosphates. Dissolved phosphorus and/or decomposed organic matter, carried into the cave by water, may well account for the presence of this element. Aluminum is instead likely related to the presence of clay minerals documented in the cave (kaolinite and pyrophyllite). The association with alunite suggests a highly acidic minerogenetic environment (Khalaf 1990; Wray 2011).

Acknowledgments

This research is supported by the Italian Ministero dell'Istruzione Università e Ricerca (MIUR). We kindly thank Pier Luigi Fabbri for his valuable support in collecting ESEM images at the Centro Interdipartimentale Grandi Strumenti (CIGS), Università di Modena e Reggio Emilia. Associate Editor Fernando Colombo, Annibale Mottana, and an anonymous reviewer significantly contributed to increase the quality of this contribution by sharing constructive remarks. This research was developed within the "Tepui Project" of "La Venta Esplorazioni Geografiche." We would like to thank all our Venezuelan collaborators, most of all Raul Arias Betancourt and Freddy Vergara Castro, for their logistic support in Venezuela. The finding of the new mineral was possible thanks to the collaboration with "In Parques Venezuela," "Raul Helicópteros," and "Elements Adventure." The expedition to Chimanta has benefited from the official support of the Ambassador of the Bolivarian Republic of Venezuela in Italy, Julián Isaías Rodríguez Díaz.

References cited

Assaoudi, H., and Ennaciri, A. (1997) Vibrational spectra and structure of rare earth orthophosphates, weinschenkite type. Spectrochimica Acta Part A, 53, 895–902.

Aubrecht, R., Brewer-Carías, C., Smída, B., Audy, M., and Kovácik, L. (2008) Anatomy of biologically mediated opal speleothems in the world's largest sandstone cave Cueva Charles Brewer, Chimanta Plateau, Venezuela. Sedimentary Geology, 203, 181–195.

Beukes, G.J., Schoch, A.E., Van der Westhuizen, W.A., Bok, L.D.C., and De Bruiyn, H. (1984) Hotsonite, a new hydrated aluminum-phosphate-sulfate from Pofadder, South Africa. American Mineralogist, 69, 979–983.

Briceño, H.O., and Schubert, C. (1990) Geomorphology of the Gran Sabana, Guyana Shield, Southeastern Venezuela. Geomorphology, 3, 125–141.

Brown, I.D., and Altermatt, D. (1985) Bond-valence parameters from a systematic analysis of the inorganic crystal structure database. Acta Crystallographica, B41, 244–247.

Bruker AXS (1999) SAINT+ (version 6.01). Bruker AXS Inc, Madison, Wisconsin, U.S.A.

Burla, M.C., Caliandro, R., Camalli, M., Carrozzini, B., Cascarano, G.L., De Caro, L., Giacovazzo, C., Polidori, G., and Spagna, R. (2005) SIR2004: an improved tool for crystal structure determination and refinement. Journal of Applied Crystallography, 38, 381–388.

Colombo, F., Rius, J., Pannunzio-Miner, E.V., Pedregosa, J.C., Camì, G.E., and Carbonio, R.E. (2011) Sanjuanite: ab-initio crystal-structure solution from laboratory powder-diffraction data, complemented by FTIR spectroscopy and DT-DG analyses. Canadian Mineralogist, 49, 835–847.

De Abeledo, M.E.J., Angelelli, V., De Benyacar, M.A.R., and Gordillo, C.E. (1968) Sanjuanite, a new hydrated basic sulphate-phosphate of aluminum. American Mineralogist, 53, 1–8.

du Rietz, T. (1945) Kribergite, ett nyt mineral från Kristinebergs gruva I Västerbottens lan. Geologiska Foereningens i Stockholm Foerhandlingar, 67, 78–79 (in Swedish).

Frost, R.L., and Palmer, S.J. (2011) A vibrational spectroscopic study of the mixed anion mineral sanjuanite $Al_2(PO_4)(SO_4)(OH)\cdot 9H_2O$. Spectrochimica Acta Part A, 79, 1210–1214.

Huminicki, D.M.C., and Hawthorne, F.C. (2002) The crystal chemistry of the phosphate minerals. In M.L. Kohn, J. Rakovan, and J.M. Hughes, Eds., Phosphates, 48, 123–253. Reviews in Mineralogy and Geochemistry, Mineralogical Society of America, Chantilly, Virginia.

Khalaf, F.I. (1990) Diagenetic alunite in clastic sequences, Kuwait, Arabian Gulf. Sedimentology, 37, 155–164.

Louisnathan, S.J., Hill, R.J., and Gibbs, G.V. (1977) Tetrahedral bond length variations in sulfates. Physics and Chemistry of Minerals, 1, 53–69.

Mandarino, J.A. (1981) The Gladstone-Dale relationship: Part IV. The compatibility concept and its application. Canadian Mineralogist, 19, 441–450.

Martini, J.E.J. (2000) Dissolution of quartz and silicate minerals. In A.B. Klimchouk, D.C. Ford, A.N. Palmer, and W. Dreybrodt, Eds., Speleogenesis-Evolution of Karst Aquifers, p. 452–457. National Speleological Society, Huntsville, Alabama, U.S.A.

Mecchia, M., Sauro, F., Corongiu, C., and Crobu, V. (2009) Speleological explorations in the Chimanta massif quartzites (Gran Sabana, Venezuela). Supplement to Kur Magazine, 12, 1–16.

Peacor, D.R., Rouse, R.C., Coskren, T.D., and Essene, E.J. (1999) Destinezite ("diadochite"), $Fe_2(PO_4)(SO_4)(OH)\cdot 6H_2O$: its crystal structure and role as a soil mineral at Alum Cave Bluff, Tennessee. Clays and Clay Minerals, 47, 1–11.

Santos, J.O.S., Potter, P.E., Reis, N.J., Hartmann, L.A., Fletcher, I.R., and McNaughton, N.J. (2003) Age, source, and regional stratigraphy of the Roraima Supergroup and Roraima-like outliers in northern South America based on U-Pb geochronology. Geological Society of America Bulletin, 115, 331–348.

Sauro, F., Piccini, L., Mecchia, M., and De Waele, J. (2013) Comment on "Sandstone caves on Venezuelan tepuis: Return to pseudokarst?" by R. Aubrecht, T. Lánczos, M. Gregor, J. Schlögl, B. Smída, P. Liscák, Ch. Brewer-Carías, L. Vlcek, Geomorphology 132 (2011), 351–365. Geomorphology, 197, 190–196, http://dx.doi.org/10.1016/j.geomorph.2012.11.015.

Sheldrick, G.M. (1997) SHELX-97, program for crystal structure determination. University of Göttingen, Germany.

——— (2008) SHELXL-97—Program for the refinement of crystal structures. University of Göttigen, Germany.

Smith, D.G.W., and Nickel, E.H. (2007) A system for codification for unnamed minerals: Report of the Subcommittee for Unnamed Minerals of the IMA Commission on New Minerals, Nomenclature and Classification. Canadian Mineralogist, 45, 983–1055.

Urbani, F. (1996) Venezuelan cave minerals: A review. Boletín de la Sociedad Venezolana de Espeleología, 30, 1–13.

Wray, R.A.L. (1997) A global review of solutional weathering forms on quartz sandstones. Earth Science Reviews, 42, 137–160.

——— (2011) Alunite formation within silica stalactites from the Sydney Region, South-eastern Australia. International Journal of Speleology, 40, 109–116.

Manuscript received October 27, 2012
Manuscript accepted June 10, 2013
Manuscript handled by Fernando Colombo